Bulletin of the Seismological Society of America, Vol. 109, No. 1, pp. 424–432, February 2019, doi: 10.1785/0120180118

Ⓔ

Estimating the Orientation of Borehole Seismometers from Ambient Seismic Noise

by Josiah X. Ensing and Kasper van Wijk

Abstract The orientation of the horizontal components of borehole seismometers is unknown upon installation but is crucial information for any multicomponent seismic analysis. Here, we use ambient seismic noise (ASN) to estimate the orientation of a network of 12 seismic stations monitoring the Auckland volcanic field (AVF) in New Zealand. Eight of these stations are installed at varying depths in boreholes, whereas the remaining instruments are three short-period and one broadband surface seismic stations. Despite the variations in the station hardware and configuration, the ellipsoidal wave particle motion of Rayleigh waves extracted from ambient noise correlations between stations proves robust. When the maximum correlation between the estimates of the radial–vertical component and the (90° phase shifted) vertical–vertical component of the Rayleigh-wave signal exceeds 0.3, orientation estimates of the network stations have an average standard deviation of 11°. This value compares well to the 13° standard deviation in estimates of the horizontal orientation of the seismometers, based on the polarization of *P* waves from up to 40 earthquakes in eight years of regional earthquakes. This proves that the ambient noise surface-wave method for station-orientation estimation can be especially useful for borehole stations in regions of low seismicity or as an independent estimate to complement estimates from the *P*-wave recording of earthquakes.

Electronic Supplement: Table detailing the earthquakes that generated the *P* waves used for polarization analysis.

Introduction

Seismometers collect data to probe the internal structure of the Earth. Many record three orthogonal components of ground motion. The orientation of the components needs to be established for seismic methods, such as receiver functions (Langston, 1979; Ligorria and Ammon, 1999), body-wave polarization studies (e.g., Park and Ishii, 2018) and surface-wave studies (e.g., Mordret *et al.*, 2015), anisotropy analysis (e.g., Takeo *et al.*, 2016), and ambient seismic noise (ASN) tomography with radial and transverse components (van Wijk *et al.*, 2011; Haney *et al.*, 2012).

Surface seismometers are usually installed with one horizontal component pointing north and the other pointing east. For ocean-bottom and borehole seismometers, lack of control over the orientation during installation results in uncertainty about the orientation of the horizontal components. Most seismic installations have a (close to) vertical component. Gimballing at installation directs the vertical component up and levels the horizontal sensors to within a tenth of a degree (Liu *et al.*, 1986). Even without gimballing, the vertical sensor of a borehole seismometer is parallel to the casing, making it approximately vertical for vertical boreholes. The horizontal sensors on seismometers in this study are arranged orthogonally in the left-handed convention (i.e., H2 is oriented 90° clockwise from H1).

Traditionally, the orientation of the horizontal components of seismometers is estimated with recordings of seismic body waves (e.g., Aster and Shearer, 1991), or surface waves (e.g., Ekström and Busby, 2008), from passive (e.g., Stachnik *et al.*, 2012) or active sources (e.g., Anderson *et al.*, 1987). These orientation techniques are typically based on a polarization analysis. *P*-wave motion is in the direction of propagation (radial), and Rayleigh waves have radial and vertical displacement, whereas *S*- and Love waves have ground motion in the transverse direction. Identifying the wave type on the recording enables us to estimate the orientation of seismometer components. Scholz *et al.* (2017) apply principal-component analysis to determine the directions of particle motions of regional and teleseismic *P*- and Rayleigh waves. Aster and Shearer (1991) use polarization analysis of *P*- and *S* waves from shallow local and regional earthquakes. Stachnik *et al.* (2012) rotated recordings of Rayleigh-wave data, computed the correlation between the

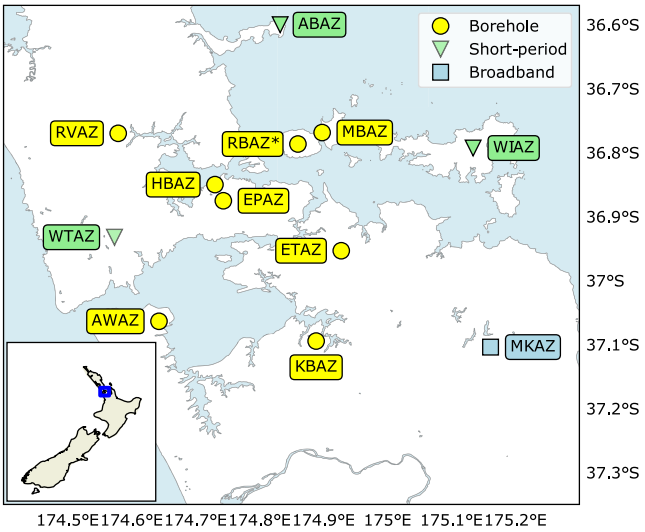

Figure 1. The Auckland volcanic seismic network (AVSN) with an additional seismometer from the University of Auckland (RBAZ*). (Inset) Location within New Zealand. The color version of this figure is available only in the electronic edition.

radial and vertical components, and subtracted the angle that resulted in the highest correlation from the station-to-event azimuth to obtain estimates of the sensor orientations. Stachnik *et al.* (2012) also rotated horizontal *P*-wave data and maximized for signal amplitude for an additional control on their estimates of the sensor orientation. Earthquakes are an abundant source of high-energy seismic data, but there is no control over the distribution of sources. Laske (1995) used polarization of long-period teleseismic surface waves from earthquakes to find that, if the azimuthal distribution of sources is poor, frequency-dependent lateral refraction biases the estimates of sensor orientation. Anderson *et al.* (1987) addressed the problem of a limited azimuthal distribution of sources by arranging explosive sources in a circle around an ocean borehole seismometer. However, active sources are often expensive and require additional equipment. Cocco *et al.* (2001) installed a surface seismometer as a reference station at the same site as a borehole seismometer. Using *P* waves from local and regional earthquakes and teleseismic surface waves, they rotated the horizontal waveform data from the borehole seismometer and optimized for the maximum cross correlation between the rotated borehole waveforms and those of the reference station data. This method requires additional equipment but reduces the limitations associated with a limited azimuthal distribution of seismic sources.

More recently, Zha *et al.* (2013) estimated the orientation of ocean-bottom seismometers with ASN as the source. This method requires no additional equipment and equates the number and distribution of sources to the distribution and number of seismic stations, which act as virtual sources. The estimates of the ocean-bottom sensor orientations proved robust in noisy environments. Zha *et al.* (2013) suggested their method may be extended to land for surface and borehole seismometers. We apply ASN orientation to a network of mixed surface and borehole seismometers that monitor the Auckland volcanic field (AVF) in New Zealand. Auckland experiences high-amplitude ASN from the surrounding waters but experiences relatively low local earthquake seismicity. We validate our results by comparing them to estimates from *P*-wave polarization of regional earthquakes associated with the boundary between the Pacific and Australian plates, some 400 km away. For both methods, estimates of orientation were computed using Python scripts that depended heavily on ObsPy (Beyreuther *et al.*, 2010).

Table 1
Depths of Borehole Seismometers

Seismometer	Depth (m)
AWAZ	371
EPAZ	383
ETAZ	347
HBAZ	380
KBAZ	160
MBAZ	96
RBAZ	50
RVAZ	250

The Auckland Volcano Seismic Network

The active AVF consists of more than 50 volcanoes in Auckland, New Zealand, a city containing one-third of the nation's population. Seismic data from the Auckland volcano seismic network (AVSN, Fig. 1), a network set up to detect volcanic tremor, are publicly available through the GeoNet project (Petersen *et al.*, 2011, see Data and Resources). The AVSN consists of seven extreme short-period borehole seismometers (Duke Malin [2 Hz]), three extreme short-period surface seismometers (two Lennartz LE-3Dlite MkIII [1 Hz], 1 Mark L4C [1 Hz]), and one broadband seismometer (Güralp CMG-3ESP). The University of Auckland installed an additional extreme short-period borehole seismometer (Duke Malin [2 Hz]) on Rangitoto Island (RBAZ). Most of these seismometers have three orthogonal sensors, but station WTAZ only has a vertical sensor. The depths of the borehole seismometers range from 50 to 383 m (Table 1), but the orientations of the horizontal components of these stations are unknown. Multicomponent seismic methods, such as *P*- and *S*-wave tomography, receiver functions, and ASN tomography could contribute significant additional information about the structure of the lithosphere beneath the AVF. However, the orientation of the horizontal components must be known before such methods can be applied to data from this network.

Methods

In the following, we introduce two methods to orient the horizontal components of a borehole seismometer.

ASN

Cross correlation of ASN can be used to estimate the Green's tensor between a pair of seismometers (Shapiro and Campillo, 2004). Each component of the Green's tensor represents seismic signal at a seismometer at location $\mathbf{x}$, as if a seismic event occurred at location $\mathbf{x}'$ (after van Wijk *et al.*, 2011)

$$\sum_k u_i(\mathbf{x}', t) * u_j(\mathbf{x}, t) \approx G_{ij}(\mathbf{x}, \mathbf{x}', t) + G_{ij}(\mathbf{x}, \mathbf{x}', -t), \quad (1)$$

in which u is the recorded wavefield, i and j represent sensor directions for virtual source and detector, the $*$ denotes cross correlation, and $G_{ij}(\mathbf{x}, \mathbf{x}', t)$ is the Green's function in direction i at location $\mathbf{x}$, due to an impulse in the j direction at $\mathbf{x}'$. In seismology, the correlation of wavefields containing ASN has proven effective in extracting surface-wave information about the Earth (Lin *et al.*, 2007; Moschetti *et al.*, 2007; Fry *et al.*, 2010; Behr *et al.*, 2011; Mordret *et al.*, 2015).

In a laterally homogeneous and isotropic medium, Rayleigh-wave ground motion is elliptical. This means that seismic signals emerge on the radial–radial, radial–vertical, vertical–radial, and vertical–vertical components of the Green's tensor. Because of the ellipticity, ground motion in the radial direction is 90° out of phase to the motion in the vertical direction, so that the Hilbert transform of G_{zz} is in phase with G_{rz}

$$G_{rz}(\mathbf{x}, \mathbf{x}', t) \propto H[G_{zz}(\mathbf{x}, \mathbf{x}', t)]. \quad (2)$$

Zha *et al.* (2013) take advantage of these Rayleigh-wave properties by applying a polarization technique to Rayleigh-wave signal retrieved from ASN recorded by ocean-bottom seismometers. This technique finds the azimuth that maximizes the correlation between G_{rz} and $H[G_{zz}]$. Here, we estimate the orientations of the surface seismometers and borehole seismometers in the AVSN using this technique.

We rotate the horizontal components of the waveforms clockwise by the azimuth of the "source" station from the "receiver" station (Fig. 2) and compute the cross-correlation functions (CCFs). G_{zz} is estimated from the vertical components of the station pair (Fig. 3a). We then rotate the horizontal–vertical Green's functions (G_{1z} and G_{2z}, see Fig. 3b,c) into radial–vertical G_{rz} (Fig. 3e) and transverse–vertical G_{tz} (Fig. 3f), respectively, with the following workflow. The Hilbert transform of G_{zz} causes a phase shift of 90°, and we compare this to rotations of G_{1z} and G_{2z} anticlockwise in 1° steps through angles 0°–360° (after Stachnik *et al.*, 2012; Zha *et al.*, 2013)

$$\tilde{G}_{rz}(\theta) = G_{1z}\cos(\theta) - G_{2z}\sin(\theta). \quad (3)$$

We evaluate the effectiveness of the rotation with a weighted correlation between $H(G_{zz})$ and $\tilde{G}_{rz}(\theta)$:

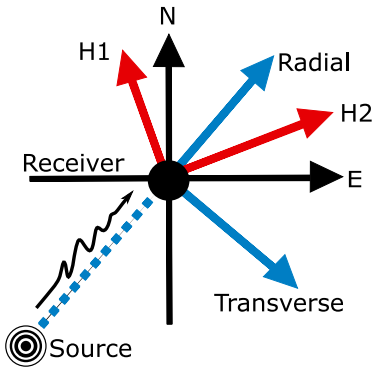

Figure 2. After Zha *et al.* (2013), seismometer components and their relation to seismic signals. North (N) and east (E) would be the conventional installation orientations. H1 and H2 represent unknown orientations. For the ambient seismic noise (ASN) orientation method, the source is a different seismic station. For the *P*-wave orientation method, the source is an earthquake. The color version of this figure is available only in the electronic edition.

$$S_{rz} = \frac{\rho(\tilde{G}_{rz}(\theta), H[G_{zz}])}{\rho(H[G_{zz}], H[G_{zz}])}, \quad (4)$$

in which $\rho(A, B)$ is the zero-lag cross correlation of two time series (A and B) and the denominator is a normalization factor. At the rotation angle θ, in which S_{rz} is maximum (Fig. 3d), $G_{1z} = \tilde{G}_{rz}(\theta) = G_{rz}$ and $G_{2z} = G_{tz}$. For pure Rayleigh-wave motion, we expect negligible signal in the transverse–vertical component G_{tz}.

We accept only estimates of the radial orientation when the maximum of $S_{rz} > 0.3$, because estimates with a lower value are indicative of noisy estimates of the Green's tensor. The circular mean and standard deviation of the remaining estimates serve as the final estimate of the azimuth of the first horizontal sensor (e.g., EH1) and the error, respectively.

P-Wave Polarization

To evaluate the ASN orientations, we estimate the orientation of the horizontal components of the seismic stations from the *P*-wave polarization of earthquake recordings. For a laterally isotropic, homogeneous medium, the initial *P*-wave ray path stays in the radial–vertical plane. Signal from the initial *P* wave will appear on the radial component (Fig. 2, Stachnik *et al.*, 2012). Maximization of the initial *P*-wave signal on one horizontal component points that component at the source.

This orientation method involves isolating the initial *P* wave and estimating the sensor orientation by polarization (Fig. 4). We manually pick the initial *P* waves and perform rotations through angles 0°–180° in 1° steps. A well-known 180° ambiguity in the resulting estimates is because the initial *P*-wave signal amplitude may be positive or negative (Stachnik *et al.*, 2012).

At each rotation, we compute the ratio A_r of the summed absolute values of the amplitude on the first unknown

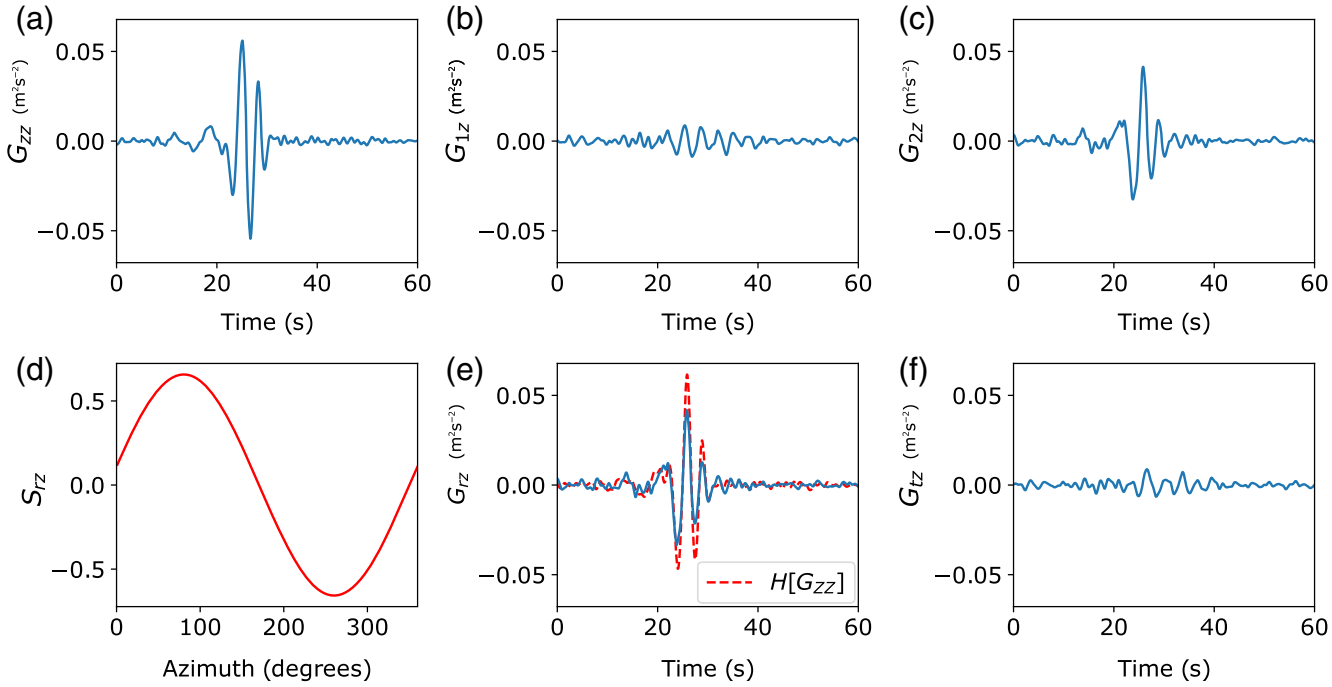

Figure 3. Components of the Green's tensor before rotation: (a) G_{zz}, (b) G_{1z}, and (c) G_{2z} for the pair of seismometers, AWAZ and ABAZ. (d) Correlation S_{rz} (equation 4) between G_{rz} and $H[G_{zz}]$ as a function of angle, with (e) G_{rz} and (f) G_{tz} as G_{1z} and G_{2z} rotated to the angle for the maximum correlation. Note the close similarity between G_{rz} and $H[G_{zz}]$. The color version of this figure is available only in the electronic edition.

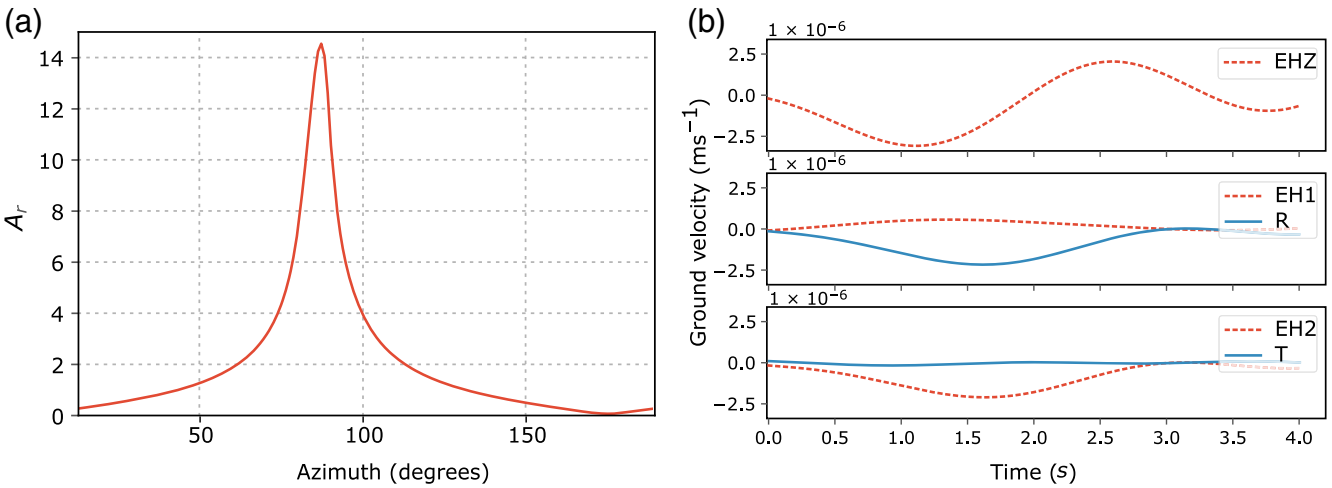

Figure 4. (a) The maximum of A_r corresponds to the orientation of the EH1 sensor in the radial direction. (b) Initial *P*-wave signal before and after a rotation maximizing A_r. (Time is measured from the start of the pick.) The color version of this figure is available only in the electronic edition.

horizontal channel, over the second (after Stachnik *et al.*, 2012)

$$A_r(\theta) = \frac{|u_1(t)\cos\theta - u_2(t)\sin\theta|}{|u_1(t)\sin\theta + u_2(t)\cos\theta|}, \qquad (5)$$

in which u_1 represents the waveform on the first unknown channel, and u_2 represents the waveform on the second channel that would be 90° clockwise of the first channel. The maximum A_r occurs where $u_r(t)$ is maximized and $u_t(t)$ is minimized (Fig. 4). Subtracting θ at the maximum A_r from the azimuth of the earthquake yields an estimate of the azimuth of the first horizontal component (e.g., EH1). We take the circular mean of the individual estimates for each earthquake as our estimate of the orientation of our horizontal components, and the standard deviation of the individual estimates give an indication of the error.

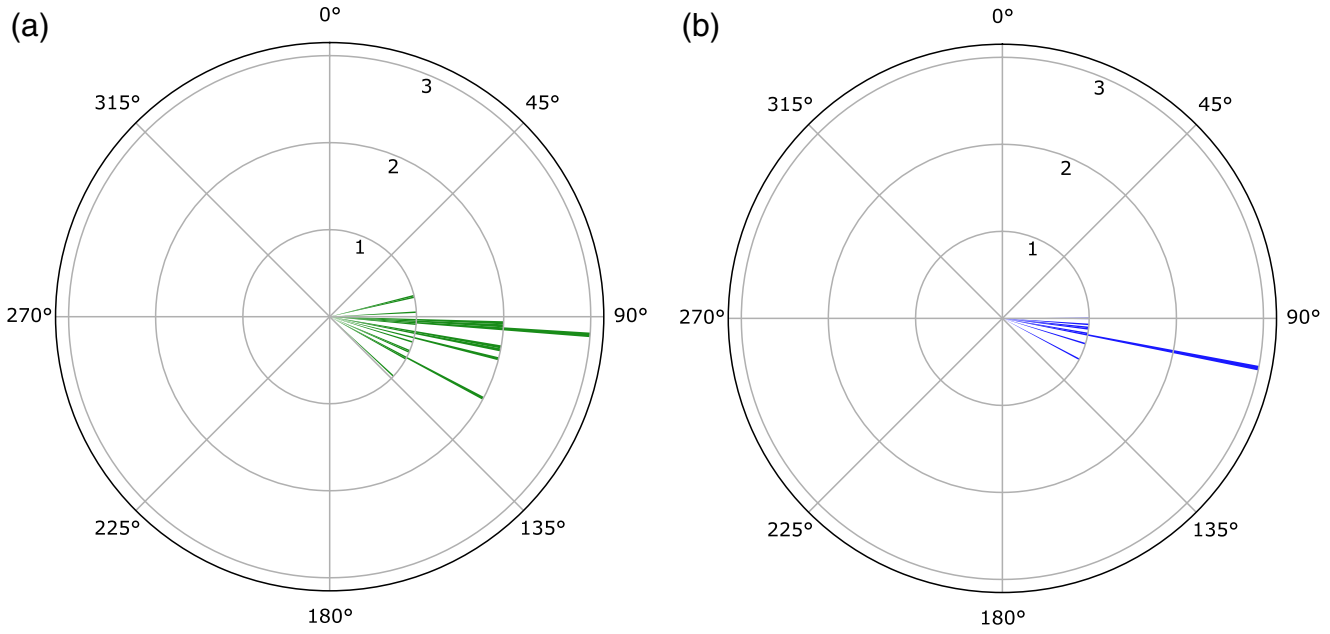

Figure 5. Example of the station-orientation estimates for Station AWAZ from (a) earthquake-generated *P* waves and (b) ambient noise. The radial axis shows the number of individual estimates. The color version of this figure is available only in the electronic edition.

Figure 5 is an example of the estimated orientation of the horizontal component H1 for station AWAZ for both methods.

Results

The AVSN is a mixed instrument network including four different sensor types. Therefore, we apply instrument corrections, filtered to 0.1–5.00 Hz, to extract the common frequency content of seismic signals in all stations.

We use MSNoise (Lecocq *et al.*, 2014) to compute CCFs that estimate the Green's tensor G_{ij} from seismic data from 200 days of data between 6 February and 15 September 2014 (Ensing *et al.*, 2017), cross correlating 1800 s time windows with a maximum lag of 120 s, as in equation (1). We 1-bit normalize the traces and whiten the frequencies. For each pair of sensors, we stack 9600 CCFs to create an average CCF. The acausal part is time reversed and summed with the causal part to increase the signal-to-noise ratio. The resulting coherent surface wave is an estimate of the surface-wave Green's function between stations. The CCFs for all components are used in equations (3) and (4) to estimate the orientation of the horizontal components of the stations of the AVSN.

To validate the ambient-noise-based estimates, we also estimate the orientations by *P*-wave polarization analysis. We apply this method to 40 regional earthquakes that occurred along the Australian and Pacific tectonic plate boundary between 2008 and 2016 (Fig. 6, and the list of earthquakes in Ⓔ Table S1, available in the electronic supplement to this article). The *P* waves from these earthquakes recorded on the stations of the AVSN are used with equation (5) to estimate the orientation of the horizontal components of these stations.

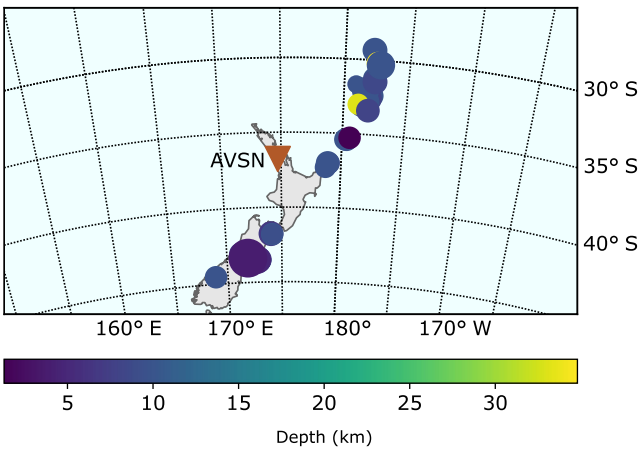

Figure 6. Epicenters of 40 earthquakes that occurred between 2008 and 2016, used in this study. The color version of this figure is available only in the electronic edition.

Surface Seismometers

The three multicomponent surface seismometers (WTAZ is only a single-component seismometer) serve as a control group, because the horizontal components of the surface stations were installed as pointing north and east. Table 2 shows the mean and standard deviation of orientation estimates for the ASN and *P*-wave methods, along with the number of station pairs and earthquakes used, respectively. The estimates of the horizontal components of the seismic stations are close to 0° (north, and the orthogonal component pointing east) for the ASN and the *P*-wave method (Table 2). The orientations estimated with the two methods are within a

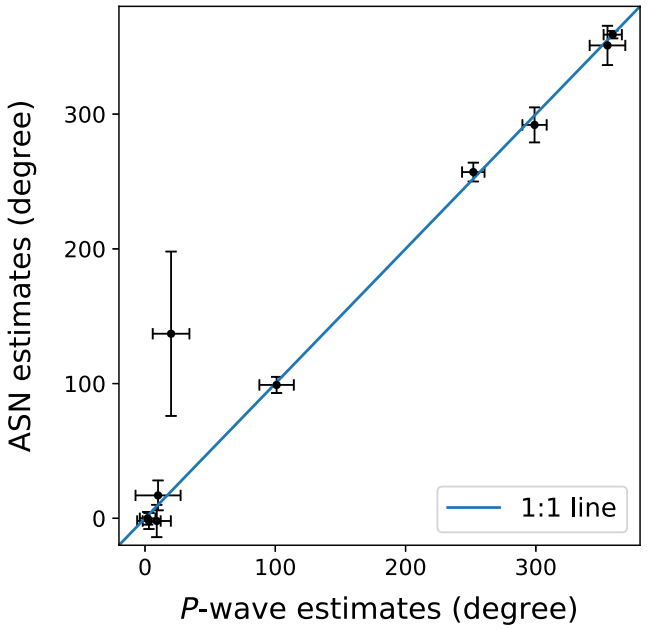

Figure 7. ASN-based station orientation estimates and *P*-wave estimates show a correlation coefficient of 0.9699 (excluding the outlier KBAZ, the correlation increases to 0.9994). The color version of this figure is available only in the electronic edition.

standard deviation of each other for all three multicomponent surface seismometers. The mean of the standard deviations for ASN-based estimates is 5° and 7° for *P*-wave polarization estimates.

Borehole Seismometers

Next, we estimated the orientation of the horizontal components of seven of eight borehole seismometers. The MBAZ seismometer was not functioning properly for the time period in 2014 that was used in this study. We overcame the 180° ambiguity in each *P*-wave-based estimate by comparing the polarity of the initial *P* wave for the borehole seismometer to the surface stations, because these have known orientations. The distance between these surface and borehole seismometers is small compared to the total length of the ray path. As a result, we can assume that, if the initial *P*-wave signal is positive on the radial component for a surface station, it will be positive for a borehole seismometer too and vice versa. The ASN estimates generally agree with *P*-wave polarization-based estimates of the orientation of the horizontal components of the borehole seismometers. Only for KBAZ do the *P* wave and ASN estimates of orientation disagree. Figure 7 shows that KBAZ is the only estimate that does not fit a 1:1 line, comparing the ASN and *P*-wave-based orientation methods. However, the ASN-based estimate of the horizontal orientation has a suspiciously large standard deviation and should therefore be rejected. The average standard deviation for the ASN estimates for the remaining six of seven borehole seismometers is 11°, contrasted with 13° for the *P*-wave polarization estimates (Table 3). There is a high correlation coefficient of 0.9994 between the estimates for the two methods for the six borehole seismometers and three surface seismometers.

Table 2
Orientation Results for Surface Stations

	ABAZ	MKAZ	WIAZ
ASN	359 ± 3	0 ± 5	358 ± 7
Pairs	11	10	11
P wave	359 ± 7	2 ± 6	3 ± 9
Events	27	20	28

ASN, ambient seismic noise.

Discussion

The consistency between the estimates of the ASN and the *P*-wave orientation methods indicates that the ASN orientation provides robust orientation measurements, even for arrays with as few as 12 seismometers. The interstation-based ASN orientation technique is beneficial for networks, for a number of reasons. Short distances between the stations ensure that there is a smaller chance of anisotropy or heterogeneity bending or multipathing waves, biasing the orientation estimates. The more stations in the network, the more estimates, from more azimuths, each orientation estimate will have. In contrast, the azimuthal distribution of seismic events used in the *P*-wave analysis spans approximately 165°, not uniformly distributed within this range. This nonuniform distribution could potentially cause a bias in the orientation estimates from *P*-wave analysis and may also be the reason for a larger standard deviation in the orientation estimates, compared to the ASN estimates. Zha *et al.* (2013) pointed out that using the ASN orientation method can increase azimuthal coverage, minimizing azimuth-related biases.

The standard deviations for borehole orientation estimates are roughly twice as large for the surface station

Table 3
Orientation Results for Borehole Seismometers

	AWAZ	EPAZ	ETAZ	HBAZ	KBAZ	RBAZ	RVAZ
ASN	99 ± 6	351 ± 15	17 ± 11	358 ± 12	137 ± 61	292 ± 13	257 ± 7
Pairs	9	8	11	8	9	9	10
P wave	101 ± 13	355 ± 14	10 ± 17	9 ± 18	340 ± 14	299 ± 9	252 ± 9
Events	27	20	31	24	16	18	24

estimates. This may be due to differences in hardware. The borehole seismometers must fit in a small-diameter borehole, potentially resulting in lower data quality than the surface stations. The boreholes' advantage of providing a quieter recording environment may be offset by the decay of Rayleigh-wave amplitude with depth (Strutt, 1885) and a reduced frequency content of the *P*-wave recordings, due to the hardware limitations. The greater standard deviation on the orientation estimates in the boreholes is consistent with the fact that 17% of the CCFs are rejected for borehole seismometers, whereas for surface stations only 6% do not meet the threshold of the maximum value of $S_{rz} > 0.3$.

These results show that the ASN method not only works for ocean-bottom sensor networks (Zha *et al.*, 2013) but even works well for mixed-instrument networks consisting of surface seismometers and borehole seismometers installed at different depths. We were able to simplify the ASN technique as introduced by Zha *et al.* (2013), because we were able to drop a secondary selection criterion based on a coherence threshold on normalized CCFs (Stachnik *et al.*, 2012; Zha *et al.*, 2013; Doran and Laske, 2017). In practice, we find that a maximum value of $S_{rz} > 0.3$ results in robust estimates of the horizontal orientation of the seismometer. The only exception to this rule was for Station KBAZ. Even though estimates of the orientation of its horizontal components had $S_{rz} > 0.3$, the results for different station pairs did not match, resulting in an anomalously high standard deviation. Because the mean did not agree with the *P*-wave method, which also had a smaller standard deviation, we concluded that the ASN result could not be trusted. Because S_{rz} involves the vertical component of the wavefield and the *P*-wave method does not, we suspect a problem with the vertical component of KBAZ.

Another advantage of the ASN method we found is that, even with 12 seismometers with four different sets of hardware, 200 days of seismic recordings resulted in better station orientation estimates than the *P*-wave method for (up to) 40 earthquakes recorded in 8 yrs. In fact, 200 days may be more than is needed. We used the CFFs of Ensing *et al.* (2017) from 200 days of seismic data. In that period, it was shown that the CCFs stabilize for this network. Future work could address the minimum time needed to obtain CCFs stable enough to estimate the station orientation. Being able to make estimates of seismometer orientation for shorter deployments will make the ASN orientation method more applicable. Ongoing maintenance and sensor replacements occur occasionally in permanent arrays, and re-analysis of the orientation may be necessary. Finding the minimum data requirements for ASN-based station orientation may help estimate orientations for seismometers with short deployment times and also help to get orientation information faster for new or changed stations in permanent arrays.

Ultimately, the seismometer orientations estimated in this study will enable seismologists to perform seismic techniques that require the waveform data to be rotated into vertical, radial, and transverse components on seismic data recorded by both the surface and the borehole seismometers in the AVSN. These additional seismic methods will shed greater light on the structure of the lithosphere beneath the AVF and contribute to our understanding of structural controls on eruptions.

Conclusions

Rayleigh waves extracted from 200 days of ASN recordings on the AVSN allow us to estimate the orientation of the horizontal components of its borehole seismometers. The AVSN is a network of four surface and eight borehole seismometers, with four different types of sensor hardware. The borehole stations are installed at a range of depths from 50 to 380 m, and still the ASN method for orientation estimation performed well. Compared with estimates based on the polarization of *P* waves recorded from up to 40 earthquakes in 8 yrs of regional earthquakes, the ASN method proves faster and more accurate, with an estimated standard deviation of 11° for ASN, versus 13° for the *P*-wave method.

Data and Resources

The seismic waveforms in this study are from the Auckland volcano seismic network (AVSN) plus one University of Auckland-operated seismometer on Rangitoto Island (RBAZ). RBAZ data are available on request (contact DEVORA at www.devora.org.nz/contact-us/, last accessed December 2018). AVSN data are publicly available through the GeoNet project (doi: 10.21420/G2WC7M). GeoNet is sponsored by the New Zealand government through its agencies: the Earthquake Commission (EQC), GNS Science, and Land Information New Zealand (LINZ). The facilities of Incorporated Research Institutions for Seismology (IRIS) Data Services, and specifically the IRIS Data Management Center, provided the earthquake catalog used for this study. IRIS Data Services are funded through the Seismological Facilities for the Advancement of Geoscience and EarthScope (SAGE) Proposal of the National Science Foundation under Cooperative Agreement EAR-1261681. The catalog of the 40 earthquakes used for *P*-wave polarization is in the Ⓔ electronic supplement. We used MSNoise (Lecocq *et al.*, 2014) to compute the cross-correlation functions (CCFs) and ObsPy (Beyreuther *et al.*, 2010) to perform the polarization analyses.

Acknowledgments

This research was supported by DEtermining VOlcanic Risk in Auckland (DEVORA) and the University of Auckland. The authors gratefully acknowledge advice and suggestions from Carolin Boese, Steven Sherburn, and Arthur Jolly. The authors thank the Eric Chael and three anonymous reviewers for their helpful remarks. The authors also gratefully acknowledge GeoNet, Incorporated Research Institutions for Seismology (IRIS), and their sponsors for providing the seismic waveform data and earthquake catalogs.

References

Anderson, P., F. Duennebier, and R. Cessaro (1987). Ocean borehole horizontal seismic sensor orientation determined from explosive charges, *J. Geophys. Res.* **92,** no. B5, 3573–3579.

Aster, R. C., and P. M. Shearer (1991). High-frequency borehole seismograms recorded in the San Jacinto Fault Zone, southern California. Part 1. Polarizations, *Bull. Seismol. Soc. Am.* **81,** no. 4, 1057–1080.

Behr, Y., J. Townend, S. Bannister, and M. K. Savage (2011). Crustal shear wave tomography of the Taupo Volcanic Zone, New Zealand, via ambient noise correlation between multiple three-component networks, *Geochem. Geophys. Geosys.* **12,** no. 3, 1–18.

Beyreuther, M., R. Barsch, L. Krischer, T. Megies, Y. Behr, and J. Wassermann (2010). Obspy: A Python toolbox for seismology, *Seismol. Res. Lett.* **81,** no. 3, 530–533.

Cocco, M., F. Ardizzoni, R. M. Azzara, L. Dall'Olio, A. Delladio, M. Di Bona, L. Malagnini, L. Margheriti, and A. Nardi (2001). Broadband waveforms and site effects at a borehole seismometer in the Po alluvial basin (Italy), *Ann. Geophys.* **44,** no. 1, 137–154, doi: 10.4401/ag-3611.

Doran, A. K., and G. Laske (2017). Ocean-bottom seismometer instrument orientations via automated Rayleigh-wave arrival-angle measurements, *Bull. Seismol. Soc. Am.* **107,** no. 2, 691–708.

Ekström, G., and R. W. Busby (2008). Measurements of seismometer orientation at USArray transportable array and backbone stations, *Seismol. Res. Lett.* **79,** no. 4, 554–561.

Ensing, J. X., K. van Wijk, and K. B. Spörli (2017). Probing the subsurface of the Auckland Volcanic Field with ambient seismic noise, *New Zeal. J. Geol. Geophys.* **60,** no. 4, 341–352.

Fry, B., F. Deschamps, E. Kissling, L. Stehly, and D. Giardini (2010). Layered azimuthal anisotropy of Rayleigh wave phase velocities in the European Alpine lithosphere inferred from ambient noise, *Earth Planet. Sci. Lett.* **297,** nos. 1/2, 95–102.

Haney, M. M., T. D. Mikesell, K. van Wijk, and H. Nakahara (2012). Extension of the spatial autocorrelation (SPAC) method to mixed-component correlations of surface waves, *Geophys. J. Int.* **191,** no. 1, 189–206.

Langston, C. A. (1979). Structure under Mount Rainier, Washington, inferred from teleseismic body waves, *J. Geophys. Res.* **84,** no. B9, 4749–4762.

Laske, G. (1995). Global observation of off-great-circle propagation of long-period surface waves, *Geophys. J. Int.* **123,** no. 1, 245–259.

Lecocq, T., C. Caudron, and F. Brenguier (2014). MSNoise, a Python package for monitoring seismic velocity changes using ambient seismic noise, *Seismol. Res. Lett.* **85,** no. 3, 715–726.

Ligorria, J. P., and C. J. Ammon (1999). Iterative deconvolution and receiver-function estimation, *Bull. Seismol. Soc. Am.* **89,** no. 5, 1395–1400.

Lin, F.-C., M. H. Ritzwoller, J. Townend, S. Bannister, and M. K. Savage (2007). Ambient noise Rayleigh wave tomography of New Zealand, *Geophys. J. Int.* **170,** no. 2, 649–666.

Liu, H.-P., R. Westerlund, J. B. Fletcher, and R. Warrick (1986). A borehole geophone leveling device, *Technical Rept., U.S. Geol. Surv*, 86–351.

Mordret, A., D. Rivet, M. Landès, and N. M. Shapiro (2015). Three-dimensional shear velocity anisotropic model of Piton de la Fournaise volcano (La Réunion Island) from ambient seismic noise, *J. Geophys. Res.* **120,** no. 1, 406–427.

Moschetti, M. P., M. H. Ritzwoller, and N. M. Shapiro (2007). Surface wave tomography of the western United States from ambient seismic noise: Rayleigh wave group velocity maps, *Geochem. Geophys. Geosys.* **8,** no. 8, 1–10.

Park, S., and M. Ishii (2018). Near-surface compressional and shear wave speeds constrained by body-wave polarization analysis, *Geophys. J. Int.* **213,** no. 3, 1559–1571.

Petersen, T., K. Gledhill, M. Chadwick, N. H. Gale, and J. Ristau (2011). The New Zealand national seismograph network, *Seismol. Res. Lett.* **82,** no. 1, 9–20.

Scholz, J.-R., G. Barruol, F. R. Fontaine, K. Sigloch, W. C. Crawford, and M. Deen (2017). Orienting ocean-bottom seismometers from P-wave and Rayleigh wave polarizations, *Geophys. J. Int.* **208,** no. 3, 1277–1289.

Shapiro, N. M., and M. Campillo (2004). Emergence of broadband Rayleigh waves from correlations of the ambient seismic noise, *Geophys. Res. Lett.* **31,** no. 7, 1–4.

Stachnik, J., A. Sheehan, D. Zietlow, Z. Yang, J. Collins, and A. Ferris (2012). Determination of New Zealand ocean bottom seismometer orientation via Rayleigh-wave polarization, *Seismol. Res. Lett.* **83,** no. 4, 704–713.

Strutt, J. W. (1885). On waves propagated along the plane surface of an elastic solid, *Proc. Lond. Math. Soc.* **1,** no. 1, 4–11.

Takeo, A., H. Kawakatsu, T. Isse, K. Nishida, H. Sugioka, A. Ito, H. Shiobara, and D. Suetsugu (2016). Seismic azimuthal anisotropy in the oceanic lithosphere and asthenosphere from broadband surface wave analysis of OBS array records at 60 Ma seafloor, *J. Geophys. Res.* **121,** no. 3, 1927–1947.

van Wijk, K., T. D. Mikesell, V. Schulte-Pelkum, and J. Stachnik (2011). Estimating the Rayleigh-wave impulse response between seismic stations with the cross terms of the Green tensor, *Geophys. Res. Lett.* **38,** no. 16, 1–4, doi: 10.1029/2011GL047442.

Zha, Y., S. C. Webb, and W. Menke (2013). Determining the orientations of ocean bottom seismometers using ambient noise correlation, *Geophys. Res. Lett.* **40,** no. 14, 3585–3590.

Appendix

Seismic Station Polarization Problems

Although most of the stations are of high quality, we found that (1) KBAZ and WTAZ have reversely polarized vertical channels, (2) the EH2 channel for EPAZ is reversely polarized, and (3) the EH1 channel for MBAZ is not performing correctly.

Reversely Polarized Channels

To investigate whether the vertical channels of the stations in the Auckland volcano seismic network (AVSN) were polarized correctly, we compared the recordings of teleseismic *P* waves (Fig. A1) from the Iquique, Chile, earthquake in 2014. The stations in the network are all within approximately a 30-km radius, so there should be consistent *P*-wave polarities across all the stations. Figure A1 shows two traces (KBAZ and WTAZ) that have negative amplitudes for the initial *P* wave, but at all the other stations it is positive. This event and several others indicate that KBAZ and WTAZ have vertical channels with reversely polarized data.

Both Rayleigh-wave and *P*-wave-based polarization estimates for EPAZ were highly variable. Renaming the channels (EH1↔EH2) resulted in estimates that were closely gathered around a mean orientation, suggesting that the horizontal channels were in some arrangement in which the channel named EH1 is 90° clockwise from EH2. We were able to determine whether this is due to channel misnaming or reverse polarization by comparing *P*-wave arrivals from shallow regional earthquakes to a reference station, such as a nearby surface station. We found that EH2 is reversely polarized (Fig. A2).

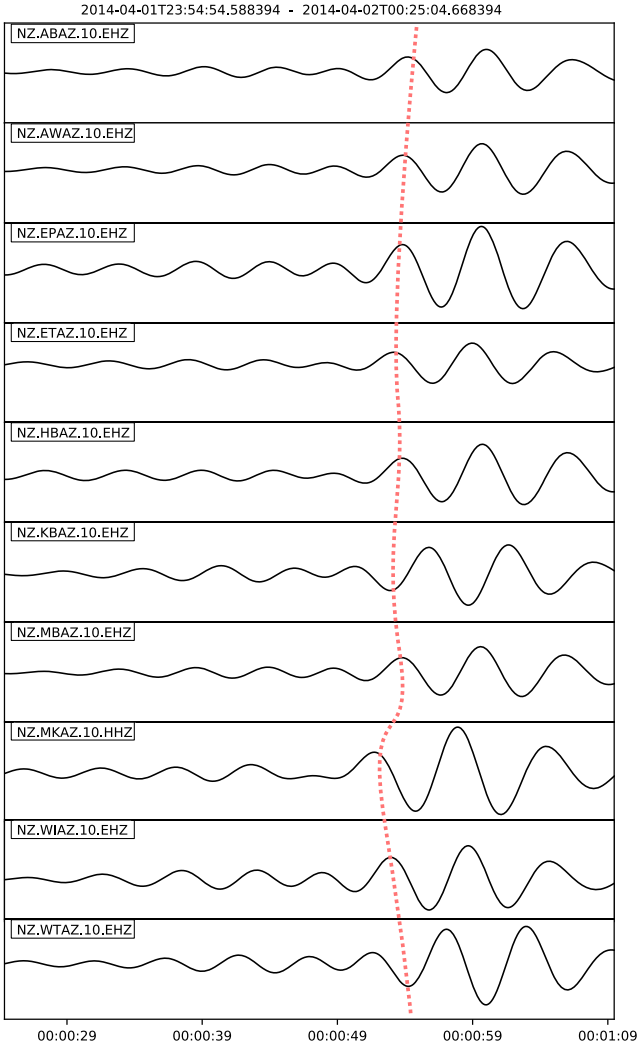

Figure A1. Waveform data from the 2014 earthquake in Iquique, Chile, for seismometers in the Auckland volcano seismic network (AVSN). The dashed line marks the *P*-wave arrival. The color version of this figure is available only in the electronic edition.

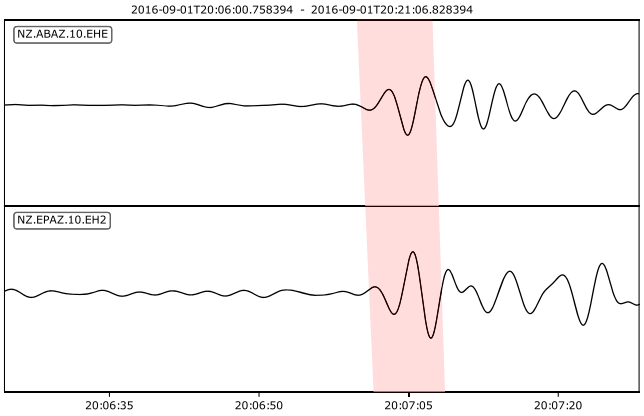

Figure A2. The initial *P*-wave signal from an earthquake (2016p661723 in the GeoNet catalog) approximately 440 km east of the Auckland volcanic field (AVF), on 1 September 2016. Note the different polarity on the ABAZ EHE and EPAZ EH2 channels in the highlighted band. The color version of this figure is available only in the electronic edition.

Finally, the EH1 channel data for MBAZ were deemed unreliable during the study period.

Some of the equipment for the KBAZ borehole seismometer was damaged in August 2014, and KBAZ and MBAZ were repaired in May 2018.

Physical Acoustics Laboratory
Department of Physics
The University of Auckland
Private Bag 92019, Auckland Mail Centre
Auckland 1142, New Zealand
josiahensing@gmail.com

Manuscript received 18 April 2018;
Published Online 11 December 2018